JOURNAL OF AIRCRAFT
Vol. 30, No. 4, July–Aug. 1993

Plume and Wake Dynamics, Mixing, and Chemistry Behind a High Speed Civil Transport Aircraft

R. C. Miake-Lye,* M. Martinez-Sanchez,† R. C. Brown,‡ and C. E. Kolb§
Aerodyne Research, Inc., Billerica, Massachusetts 01821

The environmental perturbations caused by the exhaust of a high speed civil transport (HSCT) depend on the deposition altitude and the amount and composition of the emissions. The chemical evolution and the mixing and vortical motion of the exhaust need to be analyzed to track the exhaust and its speciation as the emissions are mixed to atmospheric scales. Elements of an analytic model of the wake dynamical processes are being developed to account for the roll-up of the trailing vorticity, its breakup due to the Crow instability, and the subsequent evolution and motion of the reconnected vorticity. The concentrated vorticity is observed to wrap up the buoyant exhaust and suppress its continued mixing and dilution. The chemical kinetics of the important pollutant species will be followed throughout the plume and wake. Initial plume mixing and chemistry are calculated using an existing plume model, standard plume flowfield (SPF), with additional H/C/O, OH/SO_2, and NO_y chemistry and equilibrium H_2O condensation included. The species tracked include those that could be heterogeneously reactive on the surfaces of the condensed solid water (ice) particles when condensation occurs, and those capable of reacting with exhaust soot particle surfaces to form active contrail and/or cloud condensation nuclei (ccn).

Introduction

THE Anglo-French Concorde has shown that commercial supersonic air transportation is feasible. However, since it began commercial operations in the mid-1970s, the Concorde has served a low-volume, premium-fare market with its dozen-plus fleet. Technological advances in the intervening years have created the potential for a large fleet of more economical high speed civil transports (HSCTs) that could serve a large commercial market,[1,2] including transatlantic and Pacific rim routes in particular. With this possible development, attention has refocused[3] on the environmental impact of a much larger fleet of airplanes operating in a flight regime close to that of the Concorde.

The potential effects of these aircraft on the chemical balance in the stratosphere—and on stratospheric ozone levels in particular—are a primary environmental concern. Atmospheric modelers[4,5] have already begun to make estimates of the effects of the exhaust effluents of HSCTs on stratospheric chemistry. In doing so, a range of estimated emissions from the as-yet-undeveloped HSCT engines are deposited directly at representative altitudes and latitudes in their models. It is the purpose of the present study to provide initial estimates of chemical and physical changes that may occur between the exhaust leaving the engine and its deposition as a quiescent air mass in the stratosphere.

The exhaust from the large engines propelling a 250+ passenger supersonic airplane will be introduced into the ambient surroundings as a supersonic coflowing jet. Recent studies of supersonic mixing[6,7] indicate that supersonic convective Mach numbers suppress mixing in free shear layers, an effect that will need to be accounted for in following the initial exhaust dilution. As this initial dilution is occurring, the vortex sheet shed by the lifting surfaces of the airplane is rolling up and being concentrated in a trailing vortex pair by mutual induction of the distributed vorticity. This vorticity field will begin to affect the diluting exhaust stream and will subject the exhaust to local conditions that are sufficiently different from ambient, that significant changes in stratospheric exhaust deposition could result. The vorticity field behind a highly loaded supersonic aircraft configuration can differ dramatically from that of typical subsonic transports.

In the climatic impact assessment program (CIAP) of the early 1970s, a related study[8] was performed using contrail data collected under that program and the then-current understanding of chemistry, condensation physics, and vortex wake development. Just as supersonic flight technology has made great bounds since that time, revolutionary advances have recently been made in atmospheric chemistry. Great strides in the understanding of the stability and development of vortex wakes were being made concurrently with the CIAP program, and continued since then, and were not fully incorporated into that early study. Thus, while not starting completely anew, the present study represents a significant departure from the CIAP study and will provide a more comprehensive assessment of the chemistry and fluid physics occurring in the vortex wake.

The elements of an analytic model of these processes must include the dynamics of the vortex wake, from roll-up to breakup and dissipation, its interaction with the diluting hot exhaust, the gas-phase exhaust species chemistry, the heterogeneous chemistry occurring on condensed aerosols and soot particles, and the condensation physics governing the creation, or lack thereof, of the condensed aerosols needed for heterogeneous reactions. The stratospheric impact of the net result of all these elements will be felt through their displacement of the exhaust through vortical or buoyant transport,[9] or possible sedimentary removal of reactive species, as in polar stratospheric cloud (PSC) denitrification (and dehydration) of the polar stratosphere.[10,11] Any major chemical repartitioning of the exhaust species that is not washed out by subsequent photochemical conversions may significantly affect the composition of the chemical inputs to the global models. An understanding of the structure, motions, and persistence of the vortex wake will also be necessary for any attempt to measure the exhaust from an HSCT in flight, and for evaluating the wake hazard created for following aircraft.

Received Aug. 8, 1991; presented as Paper 91-3158 at the AIAA Aircraft Design Systems and Operations Meeting, Baltimore, MD, Sept. 23–25, 1991; revision received April 10, 1992; accepted for publication April 23, 1992.

*Principal Systems Scientist.
†Principal Research Scientist, also Associate Professor, Department of Aeronautics and Astronautics, Massachusetts Institute of Technology. Member AIAA.
‡Senior Research Scientist.
§Principal Research Scientist and President.

The analysis reported below represents the development of these several elements of a comprehensive exhaust plume/wake model for supersonic aircraft in cruise conditions. Gas-phase nozzle chemistry and plume chemistry are described in the next section and have been applied to understanding the engine exit plane conditions and the subsequent chemical evolution and condensation physics in the initial exhaust mixing region using extensions of a standard aircraft "plume" code. This chemistry will be applied in the vortex wake regime as well, as a refined model of its dynamics is finalized. The analytical basis for the vortex wake model is presented in the following section. The integration of these elements and requirements for further development are discussed in the last summary section.

Plume Mixing and Chemistry

Internal Engine Flow/Finite-Rate Kinetics Model

The internal flow for a hypothetical Mach 2.4 engine design was modeled under realistic engine operating conditions using the ODK PACKAGE code[12] for reacting flows. Emphasis was given to estimating nonequilibrium concentrations of OH and HNO_3 at the nozzle exit plane, since emission levels for these species are not currently being measured by propulsion laboratories and they were expected to strongly influence subsequent heterogeneous and homogeneous exhaust plume chemical kinetics.

The finite-rate kinetics for the internal engine flow were simulated using the reaction set consisting of 35 reversible reactions given in Table 1. These reactions were selected from kinetic data bases for hydrocarbon and nitrogen combustion chemistry. The hydrocarbon combustion reaction rate parameters were taken from a recent compilation[13] of kinetic rate data for methane combustion. Rate parameters for the reactions describing the nitrogen combustion chemistry were taken from the recent review by Miller and Bowman.[14]

To simulate the internal engine flow, equilibrium calculations were first performed to determine the chemical composition of the flow from the combustor as a function of temperature and pressure. ODK calculations were then performed in three stages to characterize the chemical and physical properties of the flow through the turbine, mixing chamber, and nozzle. For each stage, the pressure and temperature at the initial and end axial points were constrained to be consistent with representative GE engine parameters.[15] In addition, when necessary, the mixture was diluted to account for the mixing in of bypass air. Nozzle exit plane species mole fractions obtained by this method are compared against equilibrium predictions in Table 2.

Although the one-dimensional exit plume results shown in Table 2 can only approximate the chemistry and flow dynamics of anticipated HSCT engines, they do confirm that sig-

Table 1 Reaction list for HSCT internal engine flow model

Reaction	Rate constant, cm^3 molecule^{-1} s^{-1} $k = Ae^{(-E/RT)}/T^N$ A	N	E/R, K
$2H + M = H_2 + M$	1.50×10^{-29}	−1.3	0.0
$2O + M = O_2 + M$	5.20×10^{-35}	0.0	−900.0
$H + O + M = OH + M$	1.30×10^{-29}	−1.0	0.0
$OH + H + M = H_2O + M$	6.10×10^{-26}	−2.0	0.0
$CO = O + M = CO_2 + M$	1.70×10^{-33}	0.0	1,510.0
$2OH = H_2O + O$	3.50×10^{-16}	1.4	−200.0
$OH + H_2 = H_2O + H$	1.06×10^{-17}	2.0	1,490.0
$OH + H = H_2 + O$	8.10×10^{-21}	2.8	1,950.0
$OH + O = H + O_2$	7.50×10^{-10}	−0.5	30.0
$OH + CO = CO_2 + H$	2.80×10^{-17}	1.3	−330.0
$H + O_2 + M = HO_2 + M$	1.77×10^{-30}	−1.0	0.0
$H + HO_2 = 2OH$	2.80×10^{-10}	0.0	440.0
$HO_2 + H = H_2 + O_2$	1.00×10^{-10}	0.0	1,070.0
$HO_2 + H_2 = H_2O_2 + H$	5.00×10^{-11}	0.0	13,100.0
$2OH + M = H_2O_2 + M$	1.60×10^{-33}	−3.0	0.0
$2HO_2 = H_2O_2 + O_2$	3.00×10^{-12}	0.0	0.0
$H_2O_2 + OH = H_2O + HO_2$	2.90×10^{-12}	0.0	160.0
$NO + O = O_2 + N$	6.31×10^{-15}	1.0	20,820.0
$O + N_2 = NO + N$	3.02×10^{-10}	0.0	38,370.0
$NO + H = OH + N$	4.37×10^{-10}	0.0	25,370.0
$NO_2 + H = NO + OH$	5.76×10^{-10}	0.0	740.0
$NO_2 + O = NO + O_2$	1.66×10^{-11}	0.0	300.0
$N_2O + O = 2NO$	1.15×10^{-10}	0.0	13,400.0
$N_2O + H = N_2 + OH$	1.26×10^{-10}	0.0	760.0
$NO_2 + M = NO + O + M$	1.82×10^{-8}	0.0	33,000.0
$2NO_2 = 2NO + O_2$	3.31×10^{-12}	0.0	13,500.0
$HO_2 + OH = H_2O + O_2$	2.40×10^{-8}	−1.0	0.0
$HO_2 + O = OH + O_2$	2.90×10^{-11}	0.0	−200.0
$HO_2 + M = H + O_2 + M$	2.00×10^{-5}	−1.2	24,363.0
$CO + O_2 = CO_2 + O$	4.20×10^{-12}	0.0	24,000.0
$CO + HO_2 = CO_2 + OH$	2.50×10^{-10}	0.0	11,900.0
$H_2O_2 + H = H_2O + OH$	4.00×10^{-11}	0.0	2,000.0
$H_2O_2 + O = OH + HO_2$	1.60×10^{-17}	2.0	2,000.0
$CO_2 + O = CO + O_2$	2.80×10^{-11}	0.0	26,500.0
$NO_2 + OH + M = HNO_3 + M$	2.20×10^{-22}	−3.2	0.0

Table 2 Internal engine flow properties[a]

	Combustor	Turbine		Mixing chamber		Exit plane	
	Equilibrium	Equilibrium	ODK	Equilibrium	ODK	Equilibrium	ODK
p, atm	13.609	11.3	11.3	1.18	1.20	0.042	0.042
T, K	2050.0	1398.0	1383.0	1046.0	1049.0	430.0	434.0
time, s	NA	0.0033	0.0033	0.006	0.006	0.0009	0.0009
Mach no.	NA	2.17	2.17	0.26	0.26	2.85	2.84
CO	1.20×10^{-4}	1.52×10^{-7}	2.44×10^{-5}	2.02×10^{-11}	1.07×10^{-5}	5.67×10^{-31}	1.09×10^{-5}
CO_2	6.84×10^{-2}	5.94×10^{-2}	5.93×10^{-2}	3.22×10^{-2}	3.24×10^{-2}	3.22×10^{-2}	3.24×10^{-2}
H	3.26×10^{-6}	1.21×10^{-9}	1.54×10^{-6}	3.52×10^{-14}	1.49×10^{-9}	0.0	6.12×10^{-9}
HNO_3	3.28×10^{-10}	2.09×10^{-11}	6.24×10^{-10}	3.06×10^{-11}	4.46×10^{-9}	4.78×10^{-12}	4.07×10^{-8}
HO_2	1.61×10^{-6}	1.93×10^{-8}	6.97×10^{-7}	3.05×10^{-10}	1.04×10^{-7}	1.03×10^{-20}	9.77×10^{-8}
H_2	2.84×10^{-5}	7.91×10^{-8}	7.87×10^{-6}	2.70×10^{-11}	1.07×10^{-6}	4.17×10^{-28}	1.03×10^{-6}
H_2O	7.61×10^{-2}	6.62×10^{-2}	6.61×10^{-2}	3.57×10^{-2}	3.59×10^{-2}	3.57×10^{-2}	3.59×10^{-2}
H_2O_2	1.90×10^{-7}	2.61×10^{-9}	1.65×10^{-8}	7.23×10^{-11}	2.56×10^{-8}	3.66×10^{-19}	2.44×10^{-8}
NO	5.99×10^{-3}	5.54×10^{-4}	5.20×10^{-3}	4.85×10^{-5}	2.81×10^{-3}	1.66×10^{-11}	2.81×10^{-3}
NO_2	2.17×10^{-5}	3.16×10^{-6}	7.29×10^{-6}	1.76×10^{-6}	8.72×10^{-6}	1.70×10^{-9}	8.73×10^{-6}
N_2	7.47×10^{-1}	7.54×10^{-1}	7.52×10^{-1}	7.66×10^{-1}	7.68×10^{-1}	7.66×10^{-1}	7.68×10^{-1}
N_2O	1.08×10^{-6}	3.13×10^{-8}	7.89×10^{-7}	3.45×10^{-9}	4.30×10^{-7}	8.74×10^{-16}	4.30×10^{-7}
O	7.95×10^{-5}	2.76×10^{-7}	3.23×10^{-5}	2.17×10^{-10}	1.56×10^{-7}	1.22×10^{-27}	1.55×10^{-7}
OH	9.41×10^{-4}	1.93×10^{-5}	2.09×10^{-4}	1.39×10^{-7}	4.21×10^{-6}	8.13×10^{-19}	3.40×10^{-6}
O_2	9.23×10^{-2}	1.11×10^{-1}	1.08×10^{-1}	1.56×10^{-1}	1.56×10^{-1}	1.57×10^{-1}	1.56×10^{-1}

[a]Species concentrations are in mole fraction.

Table 3 Initial conditions for HSCT plume flowfield model[a]

	Exhaust	Freestream Case 1	Case 2	Case 3
Latitude		N47	N47	N85
Altitude, km		18.4	17.85	18.3
Date		June 15	January 1	January 1
p, atm		0.0734	0.0712	0.0573
T, K	5.61×10^{2}	2.19×10^{2}	2.17×10^{2}	2.05×10^{2}
v, ft/s	4.30×10^{3}	2.34×10^{3}	2.32×10^{3}	2.26×10^{3}
CO	2.37×10^{-5}	1.99×10^{-8}	1.98×10^{-8}	1.69×10^{-8}
CO_2	3.17×10^{-2}	3.50×10^{-4}	3.50×10^{-4}	3.50×10^{-4}
H	1.00×10^{-7}	1.43×10^{-20}	2.81×10^{-21}	0.0
H_2	0.0	5.18×10^{-7}	5.19×10^{-7}	5.20×10^{-7}
H_2O	3.02×10^{-2}	4.20×10^{-6}	4.20×10^{-6}	4.86×10^{-6}
HO_2	0.0	1.02×10^{-12}	3.30×10^{-13}	0.0
H_2O_2	0.0	3.51×10^{-12}	2.11×10^{-12}	0.0
N_2	0.779	0.790	0.790	0.790
NO	4.32×10^{-5}	2.43×10^{-10}	5.87×10^{-11}	0.0
NO_2	4.80×10^{-6}	8.50×10^{-10}	4.29×10^{-10}	0.0
O	0.0	6.06×10^{-13}	3.11×10^{-13}	0.0
OH	1.00×10^{-5}	1.27×10^{-13}	2.76×10^{-14}	0.0
O_2	0.159	0.210	0.210	0.210
O_3	0.0	2.48×10^{-6}	2.46×10^{-6}	3.02×10^{-6}
HNO_3	0.0	3.71×10^{-9}	3.32×10^{-9}	7.39×10^{-9}
NO_3	0.0	1.23×10^{-12}	1.71×10^{-12}	0.0
N_2O_5	0.0	3.57×10^{-10}	6.09×10^{-10}	0.0
SO_2	6.91×10^{-6}	0.0	0.0	0.0

[a]Species concentrations are in mole fraction.

nificantly nonequilibrium levels of CO, NO, NO_2, HNO_3, and OH can be anticipated at the engine nozzle exit plane. While the engine development community has long accepted the nonequilibrium nature of CO and NO_x emissions, there has been less appreciation of the high (>ppm) levels of OH emitted by gas turbine systems. The predictions presented here are consistent with the optical absorption measurements performed on the YJ93-GE-3 under stratospheric cruise conditions by McGregor et al.[16] during the CIAP program. In that study, mole fractions of exit plane OH exceeded 2×10^{-5} and 4×10^{-5} for cruise power settings equivalent to Mach 2.6 operation at 66 kft and Mach 2.0 at 55 kft.

Table 4 SPF equilibrium H_2O condensation predictions

	Case 1	Case 2	Case 3
Latitude	N47	N47	N85
Altitude, km	18.4	17.85	18.3
Date	June 15	January 1	January 1
T, K	219.3	216.7	205.2
p, atm	0.0734	0.0712	0.0573
SPF equilibrium H_2O Condensation predictions	No	No	Yes
Condensation algorithm Predictions (Ref. 21)	Never	Uncertain	Always

HSCT Plume Flow/Finite-Rate Chemical Kinetics Model

The standard plume flowfield code, SPF-2,[17] was used to characterize the chemical and physical properties of the combustion exhaust plume associated with an advanced high-altitude supersonic aircraft. Model simulations used GE parameters[15] for a hypothetical Mach 2.4 engine to specify initial exhaust emission parameters and 1990 atmospheric models[18] to specify the ambient atmospheric parameters. The SPF code was modified to include an initial estimate of the degree of H_2O condensation based on thermodynamic equilibrium. Initial examination of the plume chemistry focused on the evolution of NO_x, including an evaluation of the impact of ozone oxidation mechanisms and the percentage conversion to HNO_3, as well as SO_x oxidation cycles.

Initial Conditions

The species concentrations and thermodynamic properties used as initial conditions in model simulations of the plume chemistry and mixing are given in Table 3. This includes ambient freestream conditions and the initial conditions for the exhaust at the nozzle exit plane. Exit plane species distributions are based either on reported emission indices (g equiv/kg fuel) or on ODK calculations for the internal engine flow. An exit plane OH mole fraction of 1×10^{-5} representing a rough mean between calculated ODK value shown in Table 2 and the measurements of McGregor et al.[16] was adopted for these plume calculations. For NO_x, an emission index[19] $EI_{(NO_2)}NO_x$ of 5 was used[19,20] assuming 10% NO_2 and 90% NO on a molar basis. [The emission index for NO_x is reported as the mass equivalent of NO_2. This notation ($EI_{(NO_2)}NO_x$) resolves any possible ambiguities associated with NO_x EIs and allows the reporting convention in terms of NO_2 to be explicitly indicated. Clearly, EIs for NO and NO_2 can only be meaningfully summed to NO_x if the preceding subscripts match.] Ambient freestream conditions are given for three representative cases. These correspond to the atmospheric conditions appropriate for January 1 and June 1 at a latitude (lat) of N47 and June 1 at N85. In all three cases, the altitude (alt) was ~18 km. Ambient conditions were obtained from AER's 1990 atmospheric chemistry data base.[18]

H_2O Condensation

The SPF-2 code was modified to predict the degree of H_2O condensation during the plume expansion as part of an initial investigation into the potential role of heterogeneous kinetic processes in affecting plume chemistry. Condensation was treated using the standard vapor pressure test for thermodynamic equilibrium. It was assumed that any condensed H_2O particulates that formed would not significantly modify the flow mixing dynamics. A summary of the SPF equilibrium H_2O condensation predictions are given in Table 4 for the three case runs described by the freestream ambient conditions in Table 3. For comparison, condensation predictions based on Appleman's equilibrium, fully mixed condensation algorithm[21] are also listed in Table 4. In general, the agreement between these two approaches is good.

Plume Chemistry

The reaction set used to simulate the exhaust plume finite-rate chemical kinetics is listed in Table 5. Rate parameters for these reactions are based on a 1990 NASA evaluation[22] of the chemical kinetics data for use in stratospheric modeling. The reaction set includes reactions to describe NO_x/O_3 reactions and SO_2 oxidation kinetics.

Representative model results are presented in Table 6 which lists the plume mole fractions for nitrogen and sulfur oxides, nitric acid, hydroxyl radical, and ozone on the plume axis at axial points 500, 1000, and 2000 ft downstream of the nozzle exit plane. The speciation given in Table 6 is based on model runs using ambient atmospheric conditions appropriate for June 15 at a N47 lat (case 1 in Table 3). However, similar results were obtained for model runs with ambient conditions corresponding to January 1 at the same lat (case 2 in Table 3). The only difference was a 1.7 increase in the mole fraction of N_2O_5.

Mole fraction ratios for NO_2/NO, HNO_3/NO_x, and SO_3/SO_2 are also given in Table 6, where in this case NO_x corresponds to the sum of NO and NO_2 mole fractions. Based on this data, the SPF model calculations indicate that approximately 11% of the initial SO_2 is oxidized to SO_3. NO is oxidized to NO_2 by entrained ambient O_3. NO_2, in turn, is oxidized primarily by exhaust OH. The NO_2/NO ratio is maintained at 0.10–0.11, while approximately 5% of the NO_x is converted to HNO_3. Previous studies by Hoshizaki et al.[8] concluded that about 10–20% of the NO_x emitted is transformed to HNO_3 in the jet plume region, i.e., 1–10 s after the exhaust is emitted. Although this represents a significantly larger percentage conversion than predicted in SPF-2 simulations, the discrepancy can be explained in terms of differences in the rate parameters used. The dominant mechanism for formation of HNO_3 is

$$NO_2 + OH + M = HNO_3 + M$$

$$k = 2.2 \times (10^{-22}/T^{3.2})$$

In the early work of Hoshizaki et al.[8] this reaction was treated as a simple bimolecular reaction with a rate constant ($k = 4.8 \times 10^{-12}$) orders of magnitude larger than that adopted in the 1990 NASA evaluation[22] of the best fit to experimental data over the temperature range of interest.

The SO_3 and N_2O_5 created in the exhaust plume will react immediately on contact with contrail droplets or particles to form condensed phase H_2SO_4 and HNO_3, respectively. Exhaust gaseous HNO_3 will also condense onto contrail particles. Each of these species, gaseous SO_3, N_2O_5, and HNO_3 can also be expected to interact with exhaust soot, as can exhaust NO_2[23] and entrained atmospheric O_3,[24] to create oxidized soot surfaces capable of nucleating either exhaust contrails or atmospheric acid/water aerosols after plume mix-out. This soot surface conditioning may be an important plume chemical effect since only 1% of the soot particles formed by burning jet fuel can immediately condense water vapor at typical plume supersaturation ratios without such conditioning.[25] We plan to incorporate these heterogeneous processes in future plume chemistry models.

Table 5 Reactions list for plume chemistry/mixing model

Reaction	Rate constant, cm^3 molecule^{-1} s^{-1} $k = Ae^{(-E/RT)}/T^N$		
	A	N	E/R, K
$H + O_2 + M = HO_2 + M$	5.2×10^{-28}	1.6	0.0
$OH + O = H + O_2$	2.2×10^{-11}	0.0	240.0
$OH + H_2 = H_2O + H$	5.5×10^{-12}	0.0	−4000.0
$OH + OH = H_2O + O$	4.2×10^{-12}	0.0	−480.0
$OH + OH + M = H_2O_2 + M$	6.6×10^{-29}	0.8	0.0
$OH + HO_2 = H_2O + O_2$	4.8×10^{-11}	0.0	500.0
$OH + H_2O_2 = H_2O + HO_2$	2.9×10^{-12}	0.0	−320.0
$HO_2 + O = OH + O_2$	3.0×10^{-11}	0.0	400.0
$HO_2 + H = OH + OH$	4.2×10^{-10}	0.0	1900.0
$HO_2 + H = H_2 + O_2$	4.2×10^{-11}	0.0	−700.0
$HO_2 + HO_2 = H_2O_2 + O_2$	2.3×10^{-13}	0.0	1200.0
$H_2O_2 + O = OH + HO_2$	1.4×10^{-12}	0.0	−4000.0
$N + O_2 = NO + O$	1.5×10^{-11}	0.0	−7200.0
$N + NO = N_2 + O$	3.4×10^{-11}	0.0	0.0
$NO + O + M = NO_2 + M$	4.7×10^{-28}	1.5	0.0
$NO + HO_2 = NO_2 + OH$	3.7×10^{-12}	0.0	480.0
$NO + NO_3 = NO_2 + NO_2$	1.7×10^{-11}	0.0	300.0
$NO_2 + O = NO + O_2$	6.5×10^{-12}	0.0	240.0
$NO_2 + O + M = NO_3 + M$	8.1×10^{-27}	2.0	0.0
$NO_2 + OH + M = HNO_3 + M$	2.2×10^{-22}	3.2	0.0
$NO_2 + NO_3 + M = N_2O_5 + M$	9.9×10^{-20}	4.3	0.0
$NO_3 + O = NO_2 + O_2$	1.0×10^{-11}	0.0	0.0
$O + O_2 + M = O_3 + M$	3.0×10^{-28}	2.3	0.0
$O + O_3 = O_2 + O_2$	8.0×10^{-12}	0.0	−4120.0
$H + O_3 = OH + O_2$	1.4×10^{-10}	0.0	−940.0
$OH + O_3 = HO_2 + O_2$	1.6×10^{-12}	0.0	−1880.0
$NO + O_3 = NO_2 + O_2$	2.0×10^{-12}	0.0	−2800.0
$NO_2 + O_3 = NO_3 + O_2$	1.2×10^{-13}	0.0	−4900.0
$OH + HNO_3 = H_2O + NO_3$	7.2×10^{-15}	0.0	1570.0
$SO + O_2 = SO_2 + O$	1.4×10^{-13}	0.0	−4550.0
$SO + O_3 = SO_2 + O_2$	4.5×10^{-12}	0.0	−2340.0
$SO_2 + OH + M = HSO_3 + M$	7.5×10^{-23}	3.3	0.0
$HSO_3 + O_2 = HO_2 + SO_3$	4.0×10^{-13}	0.0	0.0
$SO + NO_2 = SO_2 + NO$	1.4×10^{-11}	0.0	0.0
$SO + OH = SO_2 + H$	8.6×10^{-11}	0.0	0.0
$SO_2 + O + M = SO_3 + M$	4.0×10^{-32}	0.0	−2000.0

Vortex Wake Dynamics

The scales and regimes involved in the dispersion of pollutants from the exhaust of stratospheric aircraft have been discussed by several authors mainly in connection with the CIAP studies in the 1970s.[26,27] The early part of the process

Table 6 Plume centerline NO_x, SO_x, and oxidizer speciation[a]

Species	Mole fractions			
	Exit plane	500 ft	1,000 ft	2,000 ft
OH	1.0×10^{-5}	1.4×10^{-7}	1.4×10^{-8}	1.9×10^{-9}
O_3	0.0	2.1×10^{-6}	2.4×10^{-6}	2.4×10^{-6}
NO	4.3×10^{-5}	6.2×10^{-6}	2.0×10^{-6}	9.4×10^{-7}
NO_2	4.8×10^{-5}	6.2×10^{-7}	2.0×10^{-7}	1.0×10^{-7}
NO_3	0.0	2.1×10^{-11}	4.5×10^{-12}	8.1×10^{-13}
N_2O_5	0.0	2.1×10^{-10}	3.2×10^{-10}	3.4×10^{-10}
HNO_3	0.0	2.4×10^{-7}	1.1×10^{-7}	5.9×10^{-8}
SO_2	6.9×10^{-6}	9.5×10^{-7}	3.0×10^{-7}	1.4×10^{-7}
SO_3	0.0	6.8×10^{-8}	3.2×10^{-8}	1.6×10^{-8}
NO_2/NO	0.11	0.10	0.10	0.11
HNO_3/NO_x	—	0.035	0.05	0.056
SO_3/SO_2	—	0.07	0.11	0.11

[a]Mach 2.4, N47, 18.4 km, June 15.

(the first hour) was described in some detail by Hoshizaki et al.,[28] who called this period "the wake regime." The first few tens of seconds of this period are characterized by the dominant role of the aerodynamic flowfield of the aircraft (first through the momentum of the jet itself, and later through the effect of the aircraft sinking vortex pair). Wake dispersion, after an ill-defined transition, is dominated by environmental effects, such as wind shear.

Based on the analysis of horizontal and vertical photographs of B-52 contrails, Ref. 28 concluded that in a first phase, called the "jet regime," the engine plumes grow by ordinary turbulent mixing to fill the recirculating vortex pair cell (of dimensions roughly 1.2 × 1.5 times the wing span). The attraction to the wing tip vortex cores was noted, but dismissed as a minor effect. After this time (~10 s), the effluent remains horizontally confined by the cell, but detrainment from the top as the cell descends leads to vertical growth. This "vortex" phase ends at about 100 s with the breakup of the vortex pair, following which wake remnants gradually lose their organized motion and ambient effects dominate. The effect of the aircraft was noticed, however, for as much as 1 h, since different aircraft lead to different dispersion rates on that time scale. This conceptual model (along with the models of Holdeman[29] and Nielsen[30] which ignored wake interactions) were later also applied to the analysis of supersonic YF-12 flight data. The interpretation of the growth of this wake is complicated by the visualization method used, as will be discussed below.

As will be discussed more fully in later sections, the depth of the pressure and temperature minima induced by the rolled-up wing-tip vortices scale as the square of the Mach number, and inversely with the square of the wing aspect ratio. Thus, what was found to be a minor effect when examining transonic aircraft, may become a very important effect for a low-aspect ratio supersonic aircraft. The horizontal densitometer scans of B-52 contrails (Hoshizaki et al.[28]) already show two peaks at the expected vortex core locations, and many other observations (e.g., photographs in Ref. 32) indicate the persistence of these two separate, well-defined and nongrowing columns of condensation material up to the time of vortex breakdown.

The extent of plume gas trapping in the low-pressure troughs caused by the vortical motion, and the degree to which exhaust gas is able to escape and be detrained from the sinking recirculating vortex pair cell, determine the effectiveness of the vortex confinement and mixing suppression. These factors are strongly dependent on the relative spanwise location of the engines and the vortex cores, and also on the "attraction" of these cores, as measured by their pressure trough depth. The trapped and the detrained portions of the exhaust gas follow very different dilution and cooling histories. While the classical Appleman[21] treatment (isobaric mixing of effluent and ambient air) should be applicable to the detrained portion, the portion captured by the vortex cores may undergo significantly lower temperatures during mixing, due to adiabatic expansion into the low pressure of the core. Since, to begin with, stratospheric conditions of interest are typically within ±10°C of the Appleman contrail threshold, these deviations may well initiate ice formation in the cores under conditions for which contrails would not be predicted ordinarily. In addition, the trapped gas dilutes at a much reduced rate, and this may provide ice growth times and/or chemical reaction times much longer than otherwise expected.

Given the stronger confining effect of the vortex cores in a supersonic (as compared to a transonic) aircraft, it is not even clear whether substantial detrainment from the descending vortex pair cell is to be expected in the supersonic case. If vertical detrainment were either absent or strongly reduced, the morphology of the effluent distribution at the end of the vortex wake would be quite different from what has been accepted since the studies in the 1970s. In the YF-12 data of Ref. 31, there was little vertical growth in the wake regime, amounting to as little as $\frac{1}{4}$ of that predicted by the "detrainment" model of Ref. 28. Unfortunately, interpretation of these supersonic cruise data is complicated by the fact that the measurement was based on in-flight fuel dumps from the aircraft centerline. Only those portions of the dump which mixed with the warm buoyant plume would be subject to vortex capture, leaving the rest free to detrain.

An additional difference between conventional and supersonic aircraft wakes must be mentioned here. For most conventional aircraft, the vortex pair becomes unstable and breaks up into irregular vortex rings at about the same time as its vertical motion is arrested by the stable atmospheric stratification. Organized vertical motion would in any case be ended by the latter effect at this point, and the coincidence has led to an identification of "vortex pair breakup" with "vorticity dissipation." In the supersonic case, however, the vortex pair has more vertical momentum, and its vertical motion will continue (in the form of vortex rings) well after the straight vortex system has broken up. This will probably lead to pollutant deposition at lower altitudes (by a few hundred meters) than expected, and also to longer than expected confinement times. The effect may also be significant in terms of wake hazards to other aircraft.

The following section, plus Appendixes A and B, provide a more detailed discussion of these effects, based on a series of simplified analytical models which are intended to approximately quantify their relative importance and scales.

Analysis

Aircraft and Vortex Parameters

Table 7 summarizes the parameters assumed for our vortex wake analysis. The airplane is a Mach number 2.4 design beginning its cruise at 17.4-km altitude. For estimates of wake properties, an elliptic loading distribution has been adopted, and the vortex roll-up distance was estimated based on Ref. 33.

The structure of the vortices after roll-up has been calculated based on the Betz-Donaldson model,[33,34] according to which, the circulation originally bound to the wing outboard of a spanwise location y_1 will end up rolled into the inner part of the trailing vortex core, within a radius r from its center—which equals the distance from y_1 to the centroid of the circulation distribution outboard of y_1. For the assumed elliptic loading, this model predicts a tangential velocity distribution near each core given by

$$\frac{v_\theta}{v} = 0.25 \frac{C_L}{AR} \sqrt{\frac{b}{r}} \tag{1}$$

where v is the flight speed, C_L the lift coefficient, AR the wing aspect ratio, b the wing span, and r the distance to the vortex core. This has been confirmed in tests,[33] and it appears to hold to radii much smaller than the classical core size estimate of Prandtl,[34] with the result that v reaches higher values near the core than expected on the basis of a model with all the vorticity concentrated in the Prandtl core. The validity of the Betz-Donaldson model has been debated,[35] and no rigorous basis for it seems to exist. We use it here simply as a convenient semiempirical device.

Using Eq. (1), several quantities of interest can be calculated. The centripetal acceleration v_θ^2/r is, using the parameters in Table 7

$$g_{\text{centripetal}} \cong (3500/r^2) \qquad \text{(in MKS units)} \tag{2}$$

With reference to Fig. 1, this gives 26 m/s² at the inboard plume location, and 73 m/s² at the outboard plume location. This shows that centripetal buoyancy effects will be strong and will compete with (perhaps dominate) those of upwards buoyancy and turbulent detrainment of effluents from the cell's edge. Notice [Eq. (1)] that the peculiar features of the

Table 7 Assumed aircraft data for wake dynamics

Wing area	$A_W = 660$ m^2	Span	$b = 39$ m
Weight (cruise)	$W = 2.76 \times 10^6$ N		
Flight altitude	$Z = 17.4$ km	Aspect ratio	$\frac{b^2}{A_W} = 2.30$
Mach no.	$M = 2.4$	Speed	$v = 708$ m/s
Atmosphere	$\rho = 0.135$ kg/m^3, $T = 217$ K, $p = 83.8$ mb		
Lift coefficient	$C_L = 0.124$		
Exhaust temperature	$T_e = 445$ K		
Fuel/air ratio	0.0155		
Airflow	$m_a = 97$ kg/s/engine		
Exhaust speed (relative)	1430 m/s		
Wake time scale	$\tau = 2\frac{AR}{C_L} = \frac{\rho v b^3}{W} = 2.04$ s		
Vorticity roll-up time	$t_{ru} \cong 1.5\tau = 3.07$ s		
Vorticity roll-up distance	$x_{ru} = vt_{ru} = 2170$ m (56 b)		
Rolled-up vortex spacing	$2\bar{y} = \frac{\pi}{4} b = 30.6$ m		
Centerline vortex circulation	$\Gamma_0 = \frac{4}{\pi}\frac{W}{\rho v b} = 943$ m^2/s		
Self-induced descent velocity	$w_0 = \frac{\Gamma_0}{2\pi(2\bar{y})} = 4.90$ m/s		
Vortex break-up time	$t_{vb} \cong 15\tau = 30.7$ s		
Vortex break-up distance	$x_{vb} = vt_{vb} = 21{,}700$ m (556 b)		

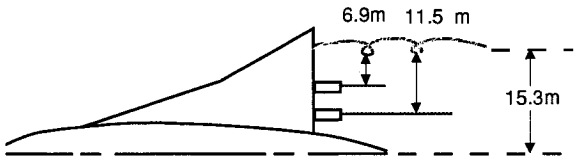

Fig. 1 Engine location with respect to rolled-up vortex core. The core is at $(\pi/4)(b/2)$ from centerline.

HSCT (small AR, high v) greatly emphasize this effect. For a transonic airplane of the same wing area, but with a lift coefficient of 0.5, and an AR of 10, $g_{\text{centripetal}}$ would be less by a factor of 17.2 at the same value of b/r. This makes plume/wake interaction a secondary issue for such aircraft, and may account for its dismissal by Hoshizaki et al.[28] and, more generally, for the lack of attention it has ellicited so far.

The pressure gradient set up by the vortex follows easily from the hydrostatic radial force balance $\partial p/\partial r = -\rho v_\theta^2/r$. From Eq. (1), and ignoring the relatively small effects of compressibility, the local depression, $\Delta p = p_\infty - p$, is seen to vary as $1/r$. Assuming adiabatic expansion, the corresponding temperature depression is found to be

$$\frac{\Delta T}{T_a} = -\frac{6(\gamma - 1)}{\pi^4}\frac{M^2 C_L^2}{AR^2}\frac{b}{r} \tag{3}$$

For the parameters of Table 7, we find $\Delta T(K) \cong -3.5/r(m)$. Once again, for typical transonic aircraft, the corresponding ΔT is less by a factor of 83, making it almost unobservable.

The vortex system is known to break up due to growth of the Crow instability (vortex bursting is unlikely at the moderate C_L of cruise). The estimate for breakup time given in Table 7 ($t_B \cong 15\tau$) is consistent with data of Ref. 36 for a quiescent atmosphere, and is 50% longer than the estimate given by Hoshizaki et al.[28] for tropospheric conditions.

Turbulent Plume Growth with Buoyancy Effects

The initial spread of the engine plumes must be controlled by turbulence generated by the plume/ambient velocity shear. However, centripetal buoyancy effects must be felt strongly, as noted, and will eventually dominate the plume dynamics. The overall dynamics is fairly complex, and we will attack it initially by considering simpler model problems. The first question is the estimation of the time after which buoyancy dominates over jet growth. To this end, we temporarily ignore the shearing of the plume by the vortex flowfield, and consider a buoyant round engine jet in the coflowing airstream. The analysis is relegated to Appendix A, and is based on the use of a turbulent diffusivity model which combines those of Prandtl[37] for a coflowing jet and of Morton et al.[38] for a rising linear plume. The resulting jet diameter is found to evolve with distance x as

$$\frac{D}{D_0} = [1 + \theta G(\xi)]^{1/3} \tag{4a}$$

where

$$\xi = x/l, \quad l = \frac{1}{19}\frac{\eta_{ov}}{1 - \eta_{ov}}\frac{c_p T_a}{g_{\text{eff}}} \tag{4b}$$

$$\theta = 0.061\frac{F l}{\rho v_a^2 D_0^3} \tag{4c}$$

$$G(\xi) = \xi\sqrt{1 + \xi^2} + \ln(\xi + \sqrt{1 + \xi^2}) \tag{4d}$$

Here, η_{ov} is the overall engine efficiency (fuel heat value to thrust power), F is the engine thrust, and D_0 is the engine nozzle diameter. The acceleration, g_{eff}, could be either the actual gravitational acceleration, or the centripetal acceleration calculated above.

By examination of Eqs. (4a–d) we can see that when $\xi << 1$, $D \cong x^{1/3}$ (jet-dominated regime), and when $\xi >> 1$, $D \cong x^{2/3}$ (buoyant plume regime). The two are nearly equivalent at $\xi = 2$. For the parameters of Table 7, and using the centripetal g for either engine, we find that $\xi = 2$ is reached when $D/D_0 = 2.17$ (outboard engine) or $D/D_0 = 2.89$ (inboard engine). Thus, by the time centripetal buoyancy be-

comes the dominant plume growth mechanism, the dilution ratio [proportinal to $(D/D_0)^2$] is about 4.7–8.3, depending on which engine is considered. For comparison, using "natural" gravity (g = 9.8 m/s^2), the crossover occurs when D/D_0 = 4.60 (dilution ratio = 21), by which time the plumes will fill a substantial fraction of the vortex cell.

The analysis above has not accounted for the effects of compressibility on turbulent jet mixing. Ref. 6 shows substantial mixing suppression when the "convective Mach number," M^* exceeds about 0.5. M^* is measured with respect to an intermediate frame in which both pressure and total pressure are equal for both streams. In the case of equal specific heat ratios, this reduces to

$$M^* = \frac{v_2 - v_1}{a_2 + a_1} \tag{5}$$

where v and a are the respective flow and sonic velocities of the two streams. In our case (Table 7) $M^* \cong 1.01$, and the initial mixing rate should be reduced by a factor f_c between 0.2 and 0.4.[6] The factor f_c will then approach unity as mixing proceeds and the relative Mach number decreases. The effect on the above analysis would be that the average f_c would multiply both θ and l.

Model for Plume-Vortex Interactions

The fluid mechanics of the turbulent buoyant jet in the flowfield of a concentrated vortex is too complex to be adequately analyzed here, but we will at least account for the salient features in an attempt to estimate the capture time of the engine exhaust into the vortex cores. The following assumptions are made:

1) The plume is convected and sheared by the (unmodified) Betz-Donaldson vortex flow. The shearing spreads the plume around a circle centered at the vortex core, at a rate proportional to the difference $v_\theta(r - D/2) - v_\theta(r + D/2)$, where r is the distance to the core and D is the transverse plume size (see Fig. 2).

2) The plume cross section grows by entrainment of ambient air, in proportion to its inward radial velocity times its projected area (Morton-Taylor-Turner model[38]). No account is taken of axial flow, except that the model is used to estimate a plume diameter as it begins to be affected by the vortex.

3) The radial motion is obtained from a momentum balance, using the centripetal buoyancy of Eq. (2).

Letting A be the plume cross section at a given time, and $\Delta\rho$ the mean density defect in the plume, mass conservation imposes

$$\frac{\mathrm{d}}{\mathrm{d}t}(A\Delta\rho) = 0 \tag{6}$$

The entrainment rate assumption gives

$$\frac{\mathrm{d}A}{\mathrm{d}t} = \alpha \Delta s v_r \tag{7}$$

where Δs is the tangential plume spread (Fig. 2), v_r is its radial velocity (inwards), and $\alpha \cong 0.94$ is chosen to correspond for the circular cylinder case to the value used in Ref. 28.

Equating the buoyancy force to the rate of momentum increase due to mass accretion gives

$$\alpha \rho_a v_r^2 \Delta s = \frac{v_\theta^2}{r} A \Delta\rho \tag{8}$$

Finally, the shearing assumption is expressed as

$$\frac{\mathrm{d}}{\mathrm{d}t}\left(\frac{\Delta s}{r}\right) = D\frac{\partial}{\partial r}\left(\frac{v_\theta}{r}\right) \tag{9}$$

where D is assumed constant.

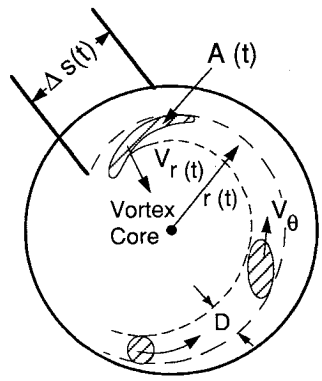

Fig. 2 Geometry of plume trapping in a plane transverse to the flight path.

Combining Eqs. (6–9) with the expression Eq. (1) for v_θ leads to a set of differential equations for which closed-form solutions can be obtained

$$\frac{vt}{b} = 0.61\alpha \frac{AR}{C_L} \frac{(r_0/b)^{5/2}}{(D_0/b)(\Delta\rho/\rho)_0} \left\{1 + 2.95\sqrt{\frac{D_0/r_0}{\alpha(\Delta\rho/\rho)_0}} \cdot \left[1 - \left(\frac{r}{r_0}\right)^{5/2}\right] - \left(\frac{r}{r_0}\right)^{5/2}\left(1 + \frac{5}{2}\ln\frac{r_0}{r}\right)\right\} \tag{10}$$

$$\frac{A}{A_0} = 1 + \frac{2}{\pi}\left(\frac{r_0}{D_0}\right)^2 \left(\left(\frac{D_0}{r_0} + \frac{\sqrt{D_0/r_0} + 1/2\beta}{\beta}\right) - \left(\frac{r}{r_0}\right)^2 \left\{\left[\sqrt{\frac{D_0}{r_0}} + \frac{\ln(r_0/r)}{\beta}\right]^2 + \frac{1}{\beta}\left[\sqrt{\frac{D_0}{r_0}} + \frac{\ln(r_0/r) + \frac{1}{2}}{\theta}\right]\right\}\right) \tag{11}$$

where

$$\beta = \frac{4}{3}\sqrt{\frac{\pi}{4\alpha}\left(\frac{\Delta\rho}{\rho}\right)_0} \tag{12}$$

also

$$\Delta\theta = \left[\sqrt{\frac{D_0}{r_0}} + \frac{\ln(r_0/r)}{\beta}\right]^2 \tag{13}$$

$$\frac{\Delta\rho/\rho}{(\Delta\rho/\rho)_0} = \frac{A_0}{A} \tag{14}$$

For application, the initial distance r_0 is 6.9 m for the outboard and 11.5 m for the inboard engine. The initial diameter D_0 and dilution [or density depression $(\Delta\rho/\rho)_0$] can only be approximately selected to account for the turbulent growth rate in the initial jet stage. A rough estimate, based on the arguments of turbulent plume growth (ignoring compressibility effects) gives (for an engine jet diameter of 2 m) initial diameters of 4 and 5 m for the outboard and inboard engine, respectively. Correspondingly, the density depressions $(\Delta\rho/\rho)_0$ are 0.122 and 0.0816, since the value at the engine face is 0.51.

Figures 3 and 4 show the subsequent evolution of plume-core distance r, angular spread $\Delta\theta$ of the sheared plume, and overall dilution ratio A/A_{jet}. Since the radial pressure gradient

intensifies towards the vortex center, the radial velocity of the plume is seen to increase with time, despite the progressive dilution. Therefore, although it is not clear what distance r to pick as the end of the "capture" process, one can make a reasonable estimate of the "capture time." For instance, Eq. (10) indicates a finite time for $r \to 0$, and this can also be seen from the downwards turning of the $r(t)$ curves in Figs. 3 and 4. Perhaps a more reasonable capture time can be chosen as that at which r equals the original plume diameter D_0 (after allowing for the initial turbulent spread) or, what is nearly equivalent, that at which the plume has been fully spread into an annulus ($\Delta\theta$ = 360 deg). This gives for the outboard engine about 90 wing spans, by which time the overall dilution (including initial turbulent growth) is about A/A_{jet} = 28. The process is slower for the inboard engine, and it takes 350 wingspans to capture that plume, with an overall dilution ratio of 56.

The basic wake time scale (Table 7) is $\tau = (2AR/C_L)(b/V)$, in terms of which roll-up takes approximately 1.5τ and break-up takes 15τ (or, for our values of AR and C_L, 56 and 560 wingspans, respectively). Therefore, we see that 1) the time for the plume capture process scales also as the basic time τ [see Eq. (10)], and 2) for both engines, the capture time is intermediate between those for roll-up and breakup, as required for validity of the modeling approach.

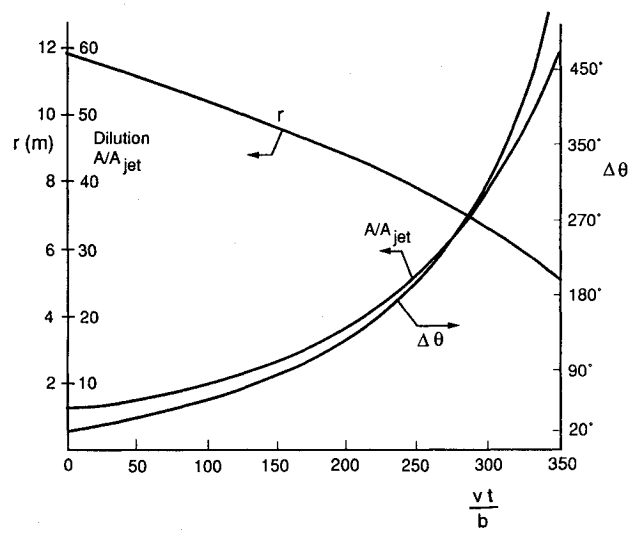

Fig. 3 Inner engine jet mixing and displacement. Initial jet diameter D_0 = 5 m, distance from vortex core r_0 = 11.5 m, and density difference $(\Delta\rho/\rho)_0$ = 0.0816.

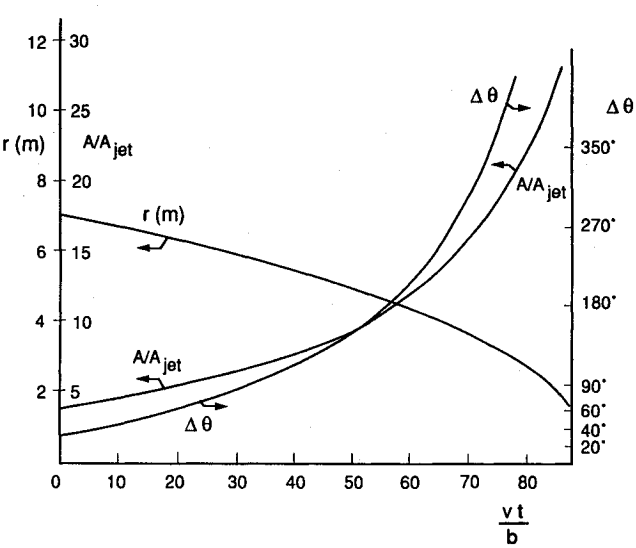

Fig. 4 Outer engine jet mixing and displacement. Initial jet diameter D_0 = 4 m, distance from vortex core r_0 = 6.9 m, and density difference $(\Delta\rho/\rho)_0$ = 0.122.

It is interesting to observe, in connection with point 1) above, that, for a given geometry and initial density defect, plume capture occurs at a fixed fraction of wake breakup time, independent of Mach number. Thus, of the two factors which are clearly different between transonic and supersonic aircraft (AR and M), only one, AR, remains to shorten the capture time in relation to wake lifetime. The reason why flight speed does not influence the time ratio is that all processes, including buoyant radial velocity and azimuthal vortex velocity, scale up together as v [see Eqs. (1) and (8)]. This fact can be exploited for setting up experimental simulations of these phenomena in water tanks. The Mach number is still important, however, in dictating deeper temperature and pressure minima in the supersonic case, and hence, strengthening centripetal buoyancy when compared to natural buoyancy. Whether or not these stronger temperature depressions lead to enhanced condensation depends on the degree of dilution ultimately achieved by the captured plume.

Last Stages of the Vortex Regime

As noted in Table 7, the wake is expected to survive as an organized cylindrical vortex cell for about 22 s. According to our analysis above, the vortex cores at breakup time may contain a large fraction of the engine exhaust, at a smaller dilution than would have been expected in the absence of the vortices, and at a temperature a few degrees lower. In attempting to extrapolate from this point, several questions arise:

1) For how much longer will the confining effects of vorticity prevent or delay plume dispersion?

2) Under what conditions will the higher plume vapor concentration and lower temperature lead to contrail formation?

3) If condensation does occur, will the confinement time be long enough for significant heterogeneous chemical interactions to occur, or for particles to grow to precipitation sizes?

Vortex Dynamics After Breakup

Unfortunately, the fluid mechanics of the broken-up vortex system is still poorly understood, and so, only very rough estimates can be made on the important question 1. Experimental and analytical stability results[36] indicate that reconnection due to growth of the Crow instability tends to produce irregular elongated ring vortices with aspect ratios of the order of 4:1. Dhanak and DeBernardinis[39] numerically followed the evolution of an elliptical ring vortex of this type and found that, after an oscillation in which the short and long axes interchange positions, the cores touch in the middle and reconnection can be expected, leading to two roughly 2:1 rings. These are then structurally stable, and oscillate as described. The time for subdivision of the original ring is (for our parameters) about 5 s.

If we can temporarily ignore the disturbing effects of wind shear, the smaller rings may continue to descend for some time, as they entrain new air by turbulent diffusion, and consequently grow in size and slow down. Glezer and Coles[40] did careful measurements of the evolution of circular turbulent rings in water, and showed that similarity exists in this motion provided a "virtual origin" is identified. In Appendix B we show that their results can be explained by means of a simple entrainment hypothesis, for which the entrainment parameter is derived from the data. As explained in Appendix B, the linear dimensions of the ring increase as $(1 + t/t_1)^{1/4}$, where $t_1 = \pi a_0/2\beta v_0$ (a_0 = initial core radius, v_0 = initial ring velocity, and $\beta \cong 0.01$). For an estimation, assume in our case, an initial ring diameter 1.5 times the linear vortex spacing (i.e., 48 m), and an initial core diameter 0.1 of the ring diameter (a_0 = 2.4 m). Since v_0 must be close to the linear vortex pair velocity of 4.9 m/s, we calculate t_1 = 76 s.

The effects of atmospheric stratification must be also considered at this point. As the air mass enclosed within the

vortex cell sinks into a stable stratified atmosphere, it will undergo adiabatic warming due to the higher pressures encountered, and will develop buoyancy. The effect of this buoyancy will eventually lead to an oscillatory vertical motion at the Brunt-Väisälä frequency

$$N = \sqrt{\frac{g}{T_a}\left(\frac{dT_a}{dz} - \frac{dT}{dz}\right)} \tag{15}$$

where $(-dT_a/dz)$ is the atmospheric lapse rate, and

$$-\frac{dT}{dz} = \frac{\gamma - 1}{\gamma}\frac{T}{H_p} \tag{16}$$

is the warming rate of the descending air (H_p is the pressure scale height of the atmosphere). However, a second effect of the descent-induced buoyancy is of interest to us. This is the production of vorticity opposite in sense to that of the wing vortices. The mechanism is clear from the two-dimensional vorticity equation

$$\frac{\partial \omega/\rho}{\partial t} + \bar{u}\cdot\nabla\left(\frac{\omega}{\rho}\right) = -\frac{1}{\rho}\nabla\left(\frac{1}{\rho}\right)\times\nabla p \tag{17}$$

The pressure gradient ∇p points vertically down, whereas, $-\nabla 1/\rho$ is concentrated on the cell's edges, and points outwards from the cell. Thus, baroclinic vorticity is generated along the cell's edges, in the sense contrary to that in the vortex cores. At the time buoyancy stops the cell's descent, the total countervorticity created is also sufficient to cancel that of the wing vortex system, although its distribution is different. We can therefore expect the vortex system, whether in the form of the undisturbed cylindrical vortex cell, or of its successor ring vortices, to vanish in the vicinity of the lowest point of the Brunt-Väisälä cycle. This occurs when $Nt \cong \pi/2$, with the vertical descent distance being then $\Delta z = -\omega_0/N$ (ω_0 = initial descent velocity). This behavior can be clearly seen in the water tank data of Ref. 36, and was also assumed by, e.g., Greene[41] in his model of wake decay.

For our parameters, with $dT_a/dz = 0$, $H_p = 6380$ m, we calculate $N = 0.0210$ rad/s, and the stratification-induced vortex destruction can be expected to happen at $t = \pi/2N = 75$ s, after a total descent of $-\Delta z = 232$ m. Notice that this is 2.4 times longer than the time required for Crow instability to occur, so that a substantial period (44 s) can be anticipated during which the ring vortices formed after breakup can retain their individuality and continue to trap the engine effluent. The amount of turbulent entrainment into the rings in this time can now be estimated from our Appendix B results. With $t_1 = 76$ s, the ring linear dimensions will increase by $(1 + 44/76)^{1/4} = 1.12$, with additional dilution by a factor $(1.12)^3 = 1.41$.

Condensation Considerations

A slight modification of the classical Appleman argument[21] concerning contrail formation will help illustrate the potential vortex effects. Assuming that each kg of burnt fuel produces 1.29 kg of water vapor and 43 MJ of heat, of which the fraction $1 - \eta_{\text{overall}} \cong 0.5$ appears as sensible heat in the plume, and that the plume dilutes continuously by isobarically mixing with air at temperature T_a and moisture w_a (g/kg), its average temperature and moisture will evolve together according to

$$T = T_a + 17.7(w - w_a) \tag{18}$$

In Fig. 5, we have represented in a T-w plot the water and ice vapor saturation lines (for an air density of 0.135 kg/m^3). The plume material will, according to Eq. (18) evolve down an inclined straight line of slope 1/17.7 towards the existing atmospheric conditions (T_a, w_a). If this line intersects the water saturation line, droplets will condense on existing condensation nuclei, and immediately freeze to form ice particles. These then persist even as the plume dilutes below the water saturation line, and will reevaporate only after the ice saturation line is recrossed.

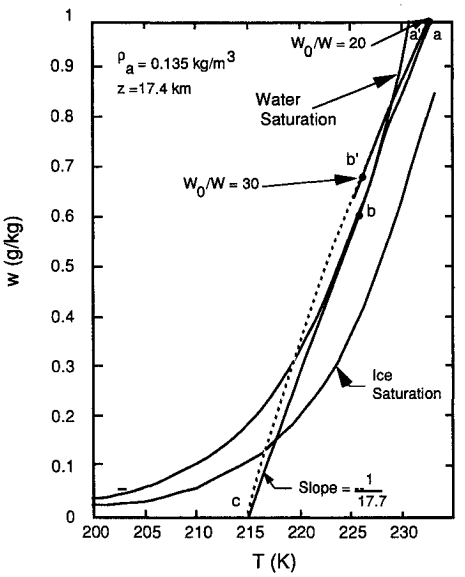

Fig. 5 Temperature—water vapor content (T-w) plane with water and ice saturation curves overlaying exhaust dilution trajectories.

In the presence of the vortex depression, however, both the ambient air and the plume gas are expanding and adiabatically cooling as they mix. Ignoring differences in the specific heat ratios, Eq. (18) must then be modified to

$$T = [T_a + 17.7(w - w_a)](p/p_a)^{(\gamma-1)/\gamma} \tag{19}$$

where $\gamma = 1.4$. Tracing the plume trajectory in the T-w plane now requires knowledge of the relationship between local pressure at the plume location and degree of dilution at that point.

As an example, consider a dry stratosphere at $T_a = 215$ K which, as Fig. 5 shows, is at the threshold for contrail formation for this air density (plume expansion along abc). Using the plume-vortex interaction model, we can calculate at each core-plume distance r the corresponding dilution ratio A/A_0 and temperature depression [Eq. (3)]. Starting from an engine-exit value $w = 20$ g/kg, we can then calculate the new plume trajectory $a'b'c$ (Fig. 5), which shows definite contrail formation. The last portion of the $a'b'c$ curve is shown dotted, as it corresponds to the poorly understood process of vortex dissipation and final dilution.

The above results indicate an increase by about 2°C of the minimum atmospheric temperature required to form a contrail. The possible global significance of this is best appreciated by reference to Fig. 6, which is the result of straightforward application of Appleman's criterion. The region labeled ALWAYS corresponds to temperatures lower than that at points like c in Fig. 5, where contrails form even in dry air. The region labeled NEVER corresponds to temperatures greater than T_b in Fig. 5, where contrails would not form even in a saturated atmosphere. By inspection of Fig. 6, the cruising altitude range (17–20 km) for a Mach 2.4 aircraft contains a significant proportion of conditions lying no more than a few degrees from the ALWAYS limit. Thus, there could be a noticeable impact on the frequency of contrail formation associated with wake-induced cooling. It may be, however, that a more significant effect than this contrail probability increase is the reduced dilution and extra confinement time provided by the wake vortices.

The size to which the contrail ice particles can grow is mainly determined by the concentration of active condensa-

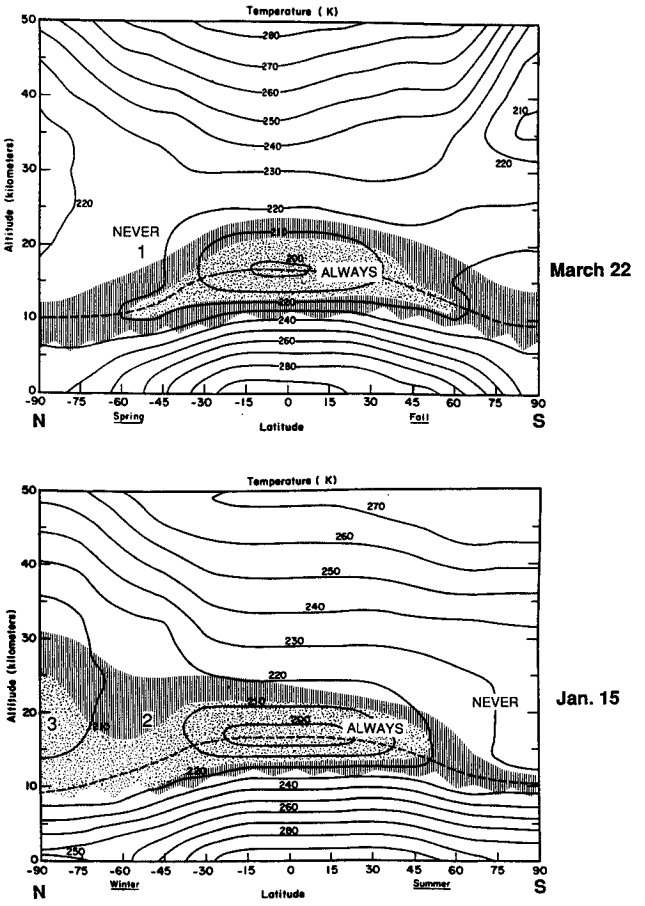

Fig. 6 Predictions using equilibrium, fully mixed condensation algorithm.

tion nuclei (cn) in the plume; kinetic limitations are less important, except perhaps for diameters over 10 μm. Unfortunately, not much is known about cn production by engines, and even less about their activation mechanisms. Knollenberg[42] sampled a Sabreliner contrail in saturated ice conditions and estimated $10^{10}/m^{-3}$ active cns at the engine exhaust plane. Rosen and Greegor[43] photoelectrically measured the total carbon particle concentration some 600-m behind an F-104 plane. Their data seem to indicate a total particle concentration of about $2.5 \times 10^{10}/m^{-3}$ extrapolated to the engine exhaust. On the other hand, Hoffmann and Rosen[44] encountered an 18-h-old SR-71 contrail which had sheared to a horizontal width of 20–90 km (but with a vertical thickness of only 200 m), and estimated emission of 3×10^{13} to 12×10^{14} m^{-3} particles greater than 0.01 μm (not necessarily all active). The fraction of all particles emitted which become active cns is also uncertain. Hallett et al.[25] measured a conversion fraction of 1 to 3% for JP-4 fuel, but the 3% level was only achieved after aging for 20 h.

From the example of Fig. 5, it is possible to have about 50% of the original vapor in the form of ice particles when the ambient temperature is near the contrail threshold. Assuming also 1.29 kg of water/kg of fuel and $p = 50$ mb, $T_{exit} = 450$ K, and letting n (m^{-3}) be the active nucleus concentration at the engine exhaust, we estimate an eventual mean particle size

$$\bar{R}\ (\mu m) \cong (10^{11}/n)^{1/3} \tag{20}$$

which, for the range of estimates of n given above implies $\bar{R}$ values between 2 and 0.06 μm. A 2-μm radius particle of pure water, falling through dry air at 210 K, would evaporate fully in about 10 s and settle no more than about 1 cm. This would indicate the lack of any contrail settling. However, two modifying factors may occur in the case of an HSCT contrail. 1) Lean-burner combustors, being developed for emissions reduction, will produce much less soot than conventional burners—perhaps by two or more orders of magnitude. Active ccn levels may be significantly lower still.[25] This may lead to ccn concentrations approaching background levels, and hence, Eq. (20) to much larger particles. 2) The extended confinement of exhaust products may lead to the formation of significant surface layers of nitric acid trihydrate (NAT) and other hydrated acid species on the ice particles [see Eqs. (21–28)]. This would lower their vapor pressure and essentially prevent reevaporation, with the result of a much larger settling distance for a given particle size.

The acid gas processing of the condensed exhaust water begins with the plume/wake chemical effects described in the previous section. The chemistry modeled there includes the formation of acid gases and their precursors (HNO_3/N_2O_5 and H_2SO_4/SO_3). These gases are formed through the scavenging of exhaust OH radicals and reaction with entrained atmospheric O_3. They are then available for heterogeneous chemistry processes that can change exhaust speciation through processes like

$$N_2O_5 + H_2O(c) \rightarrow HNO_3(c) \tag{21}$$

$$SO_3 + H_2O(c) \rightarrow H_2SO_4(c) \tag{22}$$

$$HNO_3 + H_2O(c) \rightarrow HNO_3(c) \tag{23}$$

$$H_2SO_4 + H_2O(c) \rightarrow H_2SO_4(c) \tag{24}$$

$$HCl + H_2O(c) \rightarrow HCl(c) \tag{25}$$

temporarily removing plume and atmospheric acid gases from the gas phase or setting up the liberation of reservoir atmospheric chlorine

$$ClONO_2 + H_2O(c) \rightarrow HOCl(c, g) + HNO_3(c) \tag{26}$$

$$ClONO_2 + HCl(c) \rightarrow Cl_2(g) + HNO_3(c) \tag{27}$$

$$HCl + HOCl(c) \rightarrow Cl_2(g) + H_2O(c) \tag{28}$$

The activation of plume/exhaust soot to ccn will occur on particles through their reaction with acid and oxidizing gases. In future work, we will model both this soot activation process and the kinetic nucleation and growth of contrail particles, a process which depends directly on the degree of plume/wake water vapor supersaturation, determined by the plume/wake temperature and entrainment/detrainment profiles, and the number of active condensation nuclei. Particle formation and growth through the wake dispersal regime depend on more than the simple equilibrium H_2O condensation considered in the plume mixing and chemistry section. Clearly, in this heterogeneous chemical environment, the relevant condensation phenomena determine the degree to which gravitational settling can drop the particle and its associated acid gases and exhaust particulates to lower altitudes less conducive to ozone depletion.

Summary and Conclusions

The mixing, chemistry, and condensation in the exhaust flowfield behind an HSCT were modeled as a first step in following the engine emissions to their eventual deposition in the atmosphere. Finite-rate chemistry was simulated internal to an engine for conditions that are representative of engine cycles that would be used in propelling an HSCT. This simulation was used to calculate exhaust emissions at the engine exit plane where super-equilibrium concentrations of CO, NO, NO_2, HNO_3, and OH were estimated to be present.

The exhaust emissions were followed from the engine exit plane using the standard plume flowfield code, SPF-2. The plume code was initialized using estimated emission indices

or calculated exit plane concentrations. The chemical kinetics in the plume code were upgraded for these calculations to include the chemistry for atmospherically active species. NO_x in the plume was partially converted to HNO_3 through reaction with the OH radical to leave over 5% of the NO_x as HNO_3 600-m downstream of the exhaust exit. SO_2 was also oxidized (to SO_3) so that in excess of 10% of the SO_x is available for direct conversion to H_2SO_4 upon contact with condensed H_2O.

Equilibrium water condensation was also added to the upgraded plume code to begin to include some of the condensation phenomena needed to incorporate heterogeneous chemical reactivity in the plume. Contrail formation was predicted for several altitude-latitude-season combinations. These predictions based on equilibrium H_2O condensation were consistent with the Appleman algorithm for contrail occurrence.

The SO_3, N_2O_5, and HNO_3 produced in the plume react and/or condense on the aqueous exhaust aerosols to form condensed acid solutions. These species, as well as NO_2 and entrained atmospheric O_3, can also oxidize carbonaceous soot particles emitted with the exhaust. The oxidative activation of additional nucleation sites affects the size and quantity of condensed particles available for heterogeneous chemistry. The aerosols formed and activated in the plume are subjected to the vortical flowfield in the wake of the airplane, which transports and processes the particles and gases until the wake disperses.

The vortex wake due to a Mach 2.4 airplane was analyzed to estimate its effects on the transport and mixing of the exhaust emissions. For parameters representative of a low-aspect ratio supersonic aircraft, the circulation due to the rolled-up vorticity convects and shears the exhaust plume as it wraps the exhaust gases around the core. Since the emissions are warmer than the ambient, the pressure gradient generated by the vorticity attracts the less dense gas toward the core.

The vorticity has rolled up into a concentrated trailing vortex pair within about 56 wingspans behind the airplane. This vortex wake then propagates in the stratified atmosphere until the mutual interaction between the two vortices of the pair cause reconnection and the formation of elongated elliptical vortex rings at about 560 wingspans. The "capture" of the exhaust plumes by the vortices is dependent on engine placement but, for the case considered, the outboard exhaust is captured at about 90 wingspans while the inboard exhaust takes 350 wingspans. These values depend on the airplane configuration (aspect ratio) but not on its speed (Mach number). However, the speed does affect the intensity of the vortices, their pressure field, and thus the attraction and possibly the confinement of the exhaust.

The same chemistry that occurs in the plume continues as the exhaust is transported and mixed by the vorticity in the wake until wake dispersal, with subsequent atmospheric transport. The kinetics used in calculating the evolution of the plume will be incorporated into the vortex wake model to follow the chemistry from the capture of the exhaust through the dispersal of the wake. The simplified analysis performed in the present study provides insight and estimates of the dominant processes that are occurring throughout the wake and can be used further to generate first-order estimates of the flow properties. However, it is apparent that the several individual vorticity-induced phenomena are, in fact, strongly coupled and a more detailed, presumably numerical, analysis will be necessary for quantitative estimation of the evolution of the emitted exhaust gases and their transport.

Appendix A: Buoyant Turbulent Jet in a Coflow

Consider the jet depicted in Fig. A1, issuing with some velocity and temperature excess into a parallel stream. A top-hat model of the distributions will be adopted for simplicity. The fluxes of axial momentum and of enthalpy will be conserved, while the vertical momentum flux increases with distance due to the buoyancy. The convection velocity will be approximated by the external velocity u_e. We then have

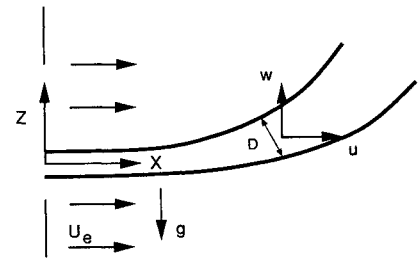

Fig. A1 Buoyant jet geometry.

$$\rho_e u_e (u - u_e) \frac{\pi D^2}{4} = F = \text{const} \tag{A1}$$

$$\rho_e u_e c_p (T - T_e) \frac{\pi D^2}{4} = Q = \text{const} \tag{A2}$$

$$\frac{\mathrm{d}}{\mathrm{d}x}\left(\rho_e u_e w \frac{\pi D^2}{4}\right) = \rho_e \frac{T - T_e}{T_e} g \frac{\pi D^2}{4} \tag{A3}$$

These equations must be supplemented by one which describes the turbulent diffusion and its effect on jet growth. In general

$$u_e \frac{\mathrm{d}D^2}{\mathrm{d}x} = 4D_t \tag{A4}$$

Where D_t is the "turbulent diffusivity." For a nonbuoyant jet, a reasonable approximation is[37] $D_t = kD(u - u_e)$, with $k \simeq 0.016$. For a nonflowing cylindrical plume, the Morton-Taylor-Turner[38] model gives $D_t = \alpha D w (\alpha \simeq 0.3)$. These two limiting forms can be interpolated by assuming

$$D_t = KD\sqrt{a^2 w^2 + (u - u_e)^2} \tag{A5}$$

where $a = \alpha/K \simeq 19$.

For the case of an engine exhaust in flight ($u_e = v$), F represents the engine's thrust, and Q its thermal energy output. Hence, if η_{ov} is the overall propulsive efficiency

$$(Fu_e/Q) = [\eta_{ov}/(1 - \eta_{ov})] \tag{A6}$$

To integrate these equations, $u - u_e$ from Eq. (A1) and w from Eq. (A3) (after integrating) are substituted into Eq. (A5) to give D_t as a function of D and x. This is then substituted in (A4), and integration gives the results quoted in Eqs. (4a–d).

Appendix B: Model for Turbulent Vortex Ring Evolution

The similarity results obtained experimentally by Glezer and Coles[40] for the growth and slowing down of a turbulent vortex ring can be understood and extrapolated by a simple model based on an entrainment hypothesis. We assume the following:

1) The vortex core cross section increases at a rate proportional to its own radius and to the ring velocity. With reference to Fig. B1

$$\frac{\mathrm{d}(\pi a^2)}{\mathrm{d}t} = \beta a v \tag{B1}$$

where β is an empirical constant.

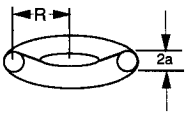

Fig. B1 Geometry of descending vortex ring.

2) Geometrical similarity is preserved, i.e., R and a grow in the same proportion

$$(a/a_0) = (R/R_0) \tag{B2}$$

3) The vertical momentum is preserved. In combination with (B2), this gives

$$a^3 v = a_0^3 v_0 \tag{B3}$$

Equations (B1), (B2), and (B3) can be combined to obtain explicit laws for the time histories of the various quantities, including the distance x traveled by the ring. Reference 37 introduced the distance x_0 and time t_0 which act as the origin for the measured self-similarity. These quantities are both negative, i.e., the "virtual origin" occurs upstream of the point of creation of the vortex ring. Our analytical results, of the same form as the data trends, are

$$(a/a_0) = (R/R_0) = [1 - (t/t_0)]^{1/4} \tag{B4}$$

$$(v/v_0) = [1 - (t/t_0)]^{-3/4} \tag{B5}$$

$$(x/x_0) = 1 - [1 - (t/t_0)]^{1/4} \tag{B6}$$

where

$$t_0 = -(\pi a_0/2\beta v_0) \tag{B7}$$

$$x_0 = -(2\pi a_0/\beta) \tag{B8}$$

In Glezer's experiments,[40] $v_0 = 128$ cm/s for the piston producing the rings. For the ring itself, we take $v_0 = 64$ m/s. Also, $R_0 = 0.953$ cm, and $a_0 \simeq 0.2R_0$, as estimated from the data. The measured virtual origin parameters were

$$t_0 = -0.44 \text{ s}, \qquad x_0 = -145 \text{ cm}$$

Using these results, Eq. (B5) gives $\beta = 0.00825$, while Eq. (B6) gives $\beta = 0.0106$. Thus, the model appears to give a reasonable description of the data using

$$\beta \simeq 0.01 \tag{B9}$$

Acknowledgments

We would like to acknowledge the support of the NASA High Speed Research Program (HSRP) Atmospheric Effects of Stratospheric Aircraft project through contract NAS1-19161. We are also grateful for the engine data provided by F. H. Krause and J. A. Matulaitis of G.E. Aircraft Engines and K. L. Hasel of Pratt & Whitney. We benefited from useful discussions with A. H. Epstein.

References

[1]"High-Speed Civil Transport Study," Boeing Commercial Airplane Co., NASA CR-4233, Sept. 1989, pp. 1–116.

[2]"Study of High-Speed Civil Transports," Douglas Aircraft Co., NASA CR-4235, Dec. 1989, pp. 1–168.

[3]Johnston, H. S., Prather, M. J., and Watson, R. T., "The Atmospheric Effects of Stratospheric Aircraft: A Topical Review," NASA Ref. Publ. 1250, Jan. 1991.

[4]Douglass, A. R., Carroll, M. A., DeMore, W. B., Holton, J. R., Isakson, I. S. A., Johnston, H. S., and Ko, M. W. K., "The Atmospheric Effects of Stratospheric Aircraft, a Current Consensus," NASA Ref. Publ. 1217, Jan. 1991.

[5]Weisenstein, D., Ko, M. K. W., Rodriguez, J. M., and Sze, N. D., "Impact of Heterogeneous Chemistry on Model-Calculated Ozone Changes Due to HSCT Aircraft," *Geophysical Research Letters*, Vol. 18, Nov. 1991, pp. 1991–1994.

[6]Papamoschou, D., and Roshko, A., "Observations of Supersonic Free Shear Layers," AIAA 24th Aerospace Science Meeting, AIAA Paper 86-0162, Reno, NV, Jan. 1986.

[7]Gutmark, E., Schadow, K. C., and Wilson, K. J., "Mixing Enhancement in Coaxial Supersonic Jets," AIAA 20th Fluid Dynamics, Plasma Dynamics, and Lasers Conf., AIAA Paper 89-1812, Buffalo, NY, June 1989.

[8]Hoshizaki, H., Anderson, L. B., Conti, R. J., Farlow, N., Meyer, J. W., Overcamp, T., Redler, K. O., and Watson, V., "Aircraft Wake Microscale Phenomena," Chap. 2 in CIAP Monograph 3, Dept. of Transportation, DOT-TST-75-53, Washington, DC, Sept. 1975.

[9]Overcamp, T. J., and Fay, J. A., "Dispersion and Subsidence of the Exhaust of a Supersonic Transport in the Stratosphere," *Journal of Aircraft*, Vol. 10, No. 12, 1973, pp. 720–728.

[10]Wofsy, S. C., Salawitch, R. J., Yatteau, J. H., McElroy, M. B., Gandrud, B. W., Dye, J. E., and Baumgardner, D., "Condensation of HNO_3 on Falling Ice Particles: Mechanism for Denitrification of the Polar Stratosphere," *Geophysical Research Letters*, Vol. 17, March Supplement, 1990, pp. 449–452.

[11]Fahey, D. W., Kelly, K. K., Kawa, S. R., Tuck, A. F., Lowenstein, M., Chan, K. R., and Heidt, L. E., "Observations of Denitrification and Dehydration in the Winter Polar Stratospheres," *Nature*, Vol. 344, March 1990, pp. 321–324.

[12]Yousefian, Y., Weinberg, M. H., and Haimes, R., "PACKAGE: A Computer Program for the Calculation of Partial Chemical Equilibrium/Partial Chemical Rate Controlled Composition of Multiphase Mixtures Under One-Dimensional Steady Flow," Aerodyne Research, Rept. ARI-RR-177, Feb. 1980.

[13]Tsang, W., and Hampson, R. F., "Chemical Kinetic Data Base for Combustion Chemistry. Part I. Methane and Related Compounds," *Journal of Physical and Chemical Reference Data*, Vol. 15, 1986, pp. 1087–1279.

[14]Miller, J. A., and Bowman, C. T., "Mechanism and Modeling of Nitrogen Chemistry in Combustion," *Progress in Energy and Combustion Science*, Vol. 15, No. 4, 1989, pp. 287–338.

[15]Matulaitis, J. A., and Krause, F. H., private communication, GE Aircraft Engines; Cincinnati, OH, 1990.

[16]McGregor, W. K., Seiber, B. L., and Few, J. D., "Concentrations of OH and NO in YJ93-GE-3 Engine Exhausts Measured In Situ by Narrow-Line UV Absorption," *Proceedings of the Second Conference on CIAP*, Nov. 1972, pp. 214–228; see also Few, J. D., and Lowry, H. S., III, "Revaluation of Nitric Oxide Concentration in Exhaust of Jet Engines and Combustors," AEDC-TR-80-65, Arnold AFB, TN, 1981.

[17]Dash, S. M., Pergament, H. S., and Thorpe, R. D., "The JANNAF Standard Plume Flowfield Model: Modular Approach, Computational Features and Preliminary Results," *Proceedings of the JANNAF 11th Plume Technology Meeting*, CPIA Pub. 306, Cambridge, MA, July 1979, pp. 345–442.

[18]Ko, M. K. W., 1990 Conditions Atmospheric Chemistry Data, Atmospheric and Environmental Research, private communication, 1990.

[19]Miake-Lye, R. C., "High-Speed Civil Transport Aircraft Emissions," *The Atmospheric Effects of Stratospheric Aircraft: A First Program Report*, NASA Reference Publication 1272, Jan. 1992, pp. 13–31.

[20]Ko, M. K. W., "Ozone Response to Aircraft Emissions: Sensitivity Studies with Two-Dimensional Models," *The Atmospheric Effects of Stratospheric Aircraft: A First Program Report*, NASA Reference Publication 1272, Jan. 1992, pp. 117–157.

[21]Appleman, H. S., "The Formation of Exhaust Condensation Trails by Jet Aircraft," *Bulletin of the American Meteorological Society*, Vol. 34, Jan. 1953, pp. 14–20; see also USAF Air Weather Service, "Forecasting Aircraft Condensation Trails," *Air Weather Service Manual 105-100*, 1960, reissued as Rept. AWS/TR-81001, Sept. 1981, Chap. 1.

[22]DeMore, W. B., Sander, S. D., Golden, D. M., Molina, M. J., Hampson, R. F., Kurylo, M. J., Howard, C. J., and Ravishankara, A. R., "Chemical Kinetics and Photochemical Data for Use in Stratospheric Modeling," Jet Propulsion Lab., JPL Publication 90-1, Pasadena, CA, Jan. 1990.

[23]Ahkter, M. S., Chughatai, R. A., and Smith, D. M., "Reaction of Hexane Soot with NO_2/N_2O_4," *Journal of Physical Chemistry*, Vol. 88, No. 22, 1984, pp. 5334–5342.

[24]Smith, D. M., Welch, W. F., Jassim, J. A., Chughatai, A. R., and Stedman, D. N., "Soot-Ozone Reaction Kinetics: Spectroscopic

and Gravimetric Studies," *Applied Spectroscopy*, Vol. 42, Nov./Dec. 1988, pp. 1473–1482.

[25]Hallett, J., Hudson, J. G., and Rogers, C. F., "Characterization of Combustion Aerosols for Haze and Cloud Formation," *Aerosol Science and Technology*, Vol. 10, 1989, pp. 70–83; see also Hudson, J. G., Hallett, J., and Rogers, C. F., "Field and Laboratory Measurements of Cloud-Forming Properties of Combustion Aerosols," *Journal of Geophysical Research*, Vol. 96, June 1991, pp. 10,847–10,859.

[26]"Propulsion Effluents in the Stratosphere," CIAP, Monograph 2, DOT-TST-75-52, NTIS, Springfield, VA, Sept. 1975, pp. 1–485.

[27]"The Stratosphere Perturbed by Propulsion Effluents," CIAP, 1975, Monograph 3, DOT-TST-75-53, NTIS, Springfield, VA, pp. 1–765.

[28]Hoshizaki, H. L., Anderson, L. B., and Conti, R. J., "High Altitude Aircraft Wake Dynamics," *Proceedings of the 2nd Conference on CIAP*, DOT-TSC-OST-73-4, Nov. 1972, pp. 263–284.

[29]Holdeman, J. D., "Dispersion and Dilution of Jet Aircraft Exhaust at High-Altitude Flight Conditions," *Journal of Aircraft*, Vol. 11, No. 8, 1974, pp. 483–487.

[30]Nielsen, J. N., Stahara, S. S., and Woolley, J. P., "Injection and Dispersion of Engine Exhaust Products by Trailing Vortices for Supersonic Flight in the Stratosphere," AIAA 12th Aerospace Science Meeting, AIAA Paper 74-42, 1974.

[31]Farlow, N. H., Watson, V. R., Lowenstein, M., and Chan, R. L., "Measurement of Supersonic Jet Aircraft Wakes in the Stratosphere," *Second International Conference on Environmental Impact of Aerospace Operations in the High Atmosphere*, American Meteorology Society, Boston, MA, 1974, pp. 53–58.

[32]Scorer, R. S., and Davenport, L. J., "Contrails and Aircraft Downwash," *Journal of Fluid Mechanics*, Vol. 43, Sept. 1970, pp. 451–464.

[33]Donaldson, C. DuP., and Bilanin, A., "Vortex Wakes of Conventional Aircraft," AGARDO-GRAPH 204, 1975.

[34]Widnall, S. E., "The Structure and Dynamics of Vortex Filaments," *Annual Review of Fluid Mechanics*, Vol. 7, 1975, pp. 141–165.

[35]Bera, R. K., "Do Inviscid Vortex Sheets Roll-up?" National Aeronautical Lab., Project Document CF 9010, Bangalore, India, May 1990.

[36]Liu, H. T., and Srnsky, R. A., "Laboratory Investigations of Atmospheric Effects on Vortex Wakes," Flow Research, Kent, WA, TR 497, Feb. 1990.

[37]Schetz, J., "Injection and Mixing in Turbulent Flow," *Progress in Astronautics and Aeronautics*, Vol. 68, 1980, pp. 52–61.

[38]Morton, B. R., Taylor, G. I., and Turner, J. S., "Turbulent Gravitational Convection from Maintained and Instantaneous Sources," *Proc. Royal Soc. London A*, Vol. 234, 1956, pp. 1–23.

[39]Dhanak, M. R., and DeBernardinis, B., "The Evolution of an Elliptic Vortex Ring," *Journal of Fluid Mechanics*, Vol. 109, Aug. 1981, pp. 189–216.

[40]Glezer, A., and Coles, "An Experimental Study of a Turbulent Vortex Ring," *Journal of Fluid Mechanics*, Vol. 211, Feb. 1990, pp. 243–283.

[41]Greene, G. C., "An Approximate Model of Vortex Decay in the Atmosphere," *Journal of Aircraft*, Vol. 23, No. 7, 1986, pp. 566–573.

[42]Knollenberg, R. G., "Measurement of the Growth of the Ice Budget in a Persisting Contrail," *Journal of Atmospheric Sciences*, Vol. 29, Oct. 1972, pp. 1367–1374.

[43]Rosen, J. M., and Greegor, R., "Jet Engine Soot Emission Measured at Altitude," *Journal of Aircraft*, Vol. 11, No. 4, 1974, pp. 243–245.

[44]Hofmann, D. J., and Rosen, J. M., "Balloon Observations of a Particle Layer Injected by a Stratospheric Aircraft at 23 km," *Geophysical Research Letters*, Vol. 5, June 1978, pp. 511–514.